# Radiation Lobe Decomposition for Directivity Patterns

(article starts on next page)

# Radiation Lobe Decomposition for Directivity Patterns

Thomas Deppisch[1], Franz Zotter[2]

[1] *Chalmers University of Technology, Gothenburg, Sweden, Email: thomas.deppisch@chalmers.se*
[2] *University of Music and Performing Arts, Graz, Austria, Email: zotter@iem.at*

## Abstract
We propose a decomposition of sound source directivity patterns expressed by spherical harmonics coefficients into a set of radiation lobes. The method reveals the direction, magnitude and two-dimensional curvature at the peak of the radiation lobes, and facilitates novel ways for the resynthesis of modified directivities. We define Newton's method on the surface of the sphere via recurrence relations of the spherical harmonics to find the direction and amplitude of the radiation lobes. The curvatures at the peaks of the lobes are determined via the Hessian. We use the parametric description of the radiation lobes to resynthesize simplified minimum-norm directivities by neglecting low-magnitude radiation lobes and by reducing the spherical harmonics reproduction order. The decomposition approach can reveal valuable information about the directivity of musical instruments and facilitates practical trade-offs in storage and rendering of directivity patterns.

## Introduction
The directivity of a sound source has a direct influence on room acoustical parameters such as early decay time, lateral energy fraction, clarity and sound pressure level [1], and it has been shown in listening experiments that this influence leads to significant perceptual differences in auralizations. Dalenbäck, Kleiner and Svensson [2] showed that the location, direction and directivity of a loudspeaker has a significant impact on the perceived reverberation, clarity and source width. Otondo and Rindel [1] found that the frequency-dependent auralization of directivities of musical instruments influences the perceived loudness, reverberance and clarity, compared to an auralization using a frequency-independent directivity. More recent investigations tried to determine the perceptual impact of a reduction of the spatial resolution of a directivity pattern. Frank and Brandner [3] showed that a maximum spherical harmonics (SH) order of 4 is sufficient for the auralization of a concert hall with a large distance between source and listener. Similar results were obtained by Enge, Frank and Höldrich [4], showing that the perceived plausibility of the auralization of an acoustic source in a VR environment did not differ significantly between a 3rd and a 7th-order SH representation. These results show that the rendering of source directivities improves the perceptual quality of an auralization but the spatial resolution of the directivity pattern can be reduced to some extent with little or no perceivable impact.

Sound source directivities are typically measured using surrounding microphone arrays. However, poor acoustic centering of sound sources, which is in practice often unavoidable, leads to phase shifts in the microphone signals and consequently to overly complicated directivity patterns [5, 6]. Several centering algorithms that minimize the energy of high-order SH coefficients of the directivity pattern were proposed to solve the problem [6, 7, 8, 9]. As an alternative, a parametric description of directivities, such as the recently proposed directivity sample combination (DISCO) approach [10], can reduce the complexity of measured directivity patterns for rendering to an arbitrary extent. DISCO samples a directivity at uniformly-distributed and pattern-independent directions and renderes it via amplitude panning.

We propose a novel parametric method for the analysis and simplification of measured directivity patterns. In contrast to DISCO, the proposed method considers directivity-specific properties such as prominent radiation directions and facilitates the further processing and storage via an SH representation. We find the direction and amplitude of directivity peaks by defining Newton's method on the surface of the sphere and subsequently decompose the directivity into radiation lobes that are parametrized by their direction, amplitude and two-dimensional peak curvature. This parametric description then allows for a simplified resynthesis of minimum-norm directivity patterns by neglecting low-magnitude radiation lobes and reducing the SH reproduction order.

## Newton's Method Using SH Recurrences
We define Newton's method on the surface of the sphere using recurrence relations of the SHs to accurately and efficiently find the peaks in a directivity pattern. Let $\boldsymbol{\gamma}_N(\omega) = [\gamma_0^0(\omega), \ldots, \gamma_N^N(\omega)]^{\mathrm{T}}$ be a vector of the SH coefficients $\gamma_n^m(\omega)$ up to order $N$ of a sound source directivity at frequency $\omega$. For notational brevity, the frequency index $\omega$ is omitted below. The amplitude $a(\boldsymbol{\theta})$ of the directivity $\boldsymbol{\gamma}_N$ can be evaluated at any direction $\boldsymbol{\theta} = [x, y, z]^{\mathrm{T}}$ using the SH expansion $a(\boldsymbol{\theta}) = \boldsymbol{y}_N^{\mathrm{T}}(\boldsymbol{\theta})\boldsymbol{\gamma}_N$. Similar to $\boldsymbol{\gamma}_N$, the vector $\boldsymbol{y}_N(\boldsymbol{\theta}) = [Y_0^0(\boldsymbol{\theta}), \ldots, Y_N^N(\boldsymbol{\theta})]^{\mathrm{T}}$ contains the real-valued SHs $Y_n^m(\boldsymbol{\theta})$ of orders $n = [1, N]$ and degrees $m = [-n, n]$. The Newton update to find the extrema of $a(\boldsymbol{\theta})$ comprises the inverse of the Hessian $\boldsymbol{H}(\boldsymbol{\theta}_k)$ and the gradient $\boldsymbol{g}(\boldsymbol{\theta}_k)$, and is defined as

$$\boldsymbol{\theta}_{k+1} = \boldsymbol{\theta}_k - \boldsymbol{H}(\boldsymbol{\theta}_k)^{-1}\,\boldsymbol{g}(\boldsymbol{\theta}_k), \quad \boldsymbol{\theta}_{k+1} \leftarrow \boldsymbol{\theta}_{k+1}/\|\boldsymbol{\theta}_{k+1}\|. \tag{1}$$

Gradient addition theorems of the SHs [11] express the partial derivatives for each coordinate as a weighted sum of SHs that are shifted in order $n$ and degree $m$. For maximum efficiency, we propose to use real-valued SHs and the corresponding addition theorems from [12] that

follow the scheme

$$\frac{\partial}{\partial x}Y_n^m = \eta_1 Y_{n-1}^{m-1} + \eta_2 Y_{n+1}^{m-1} + \eta_3 Y_{n-1}^{m+1} + \eta_4 Y_{n+1}^{m+1},$$
(2)

$$\frac{\partial}{\partial y}Y_n^m = \eta_5 Y_{n-1}^{m-1} + \eta_6 Y_{n+1}^{m-1} + \eta_7 Y_{n-1}^{m+1} + \eta_8 Y_{n+1}^{m+1},$$
(3)

$$\frac{\partial}{\partial z}Y_n^m = \eta_9 Y_{n-1}^m + \eta_{10} Y_{n+1}^m,$$
(4)

where $\eta_1$–$\eta_{10}$ are scalar weights depending on $n$ and $m$. Due to the limited space in this contribution, we do not explicitly state the recurrence relations but refer the reader to [12].

In the following derivations, we omit the dependency of $\boldsymbol{y}_N$ on $\boldsymbol{\theta}$ to improve the readability. For each coordinate $x, y, z$, the recurrences for all SHs up to order $N$ are collected in the matrices $\boldsymbol{G}_N^x, \boldsymbol{G}_N^y, \boldsymbol{G}_N^z$, such that the gradient of $a(\boldsymbol{\theta})$ is obtained as

$$\boldsymbol{g} = \begin{bmatrix} \boldsymbol{y}_{N+1}^{\mathrm{T}} \boldsymbol{G}_N^{x\mathrm{T}} \boldsymbol{\gamma}_N \\ \boldsymbol{y}_{N+1}^{\mathrm{T}} \boldsymbol{G}_N^{y\mathrm{T}} \boldsymbol{\gamma}_N \\ \boldsymbol{y}_{N+1}^{\mathrm{T}} \boldsymbol{G}_N^{z\mathrm{T}} \boldsymbol{\gamma}_N \end{bmatrix}.$$
(5)

The Hessian of $a(\boldsymbol{\theta})$ contains all second-order derivatives

$$\boldsymbol{H} = \begin{bmatrix} h_{xx} & h_{yx} & h_{zx} \\ h_{xy} & h_{yy} & h_{zy} \\ h_{xz} & h_{yz} & h_{zz} \end{bmatrix},$$
(6)

where

$$h_{\alpha\beta} = \boldsymbol{y}_{N+2}^{\mathrm{T}} \boldsymbol{G}_{N+1}^{\alpha\mathrm{T}} \boldsymbol{G}_N^{\beta\mathrm{T}} \boldsymbol{\gamma}_N.$$
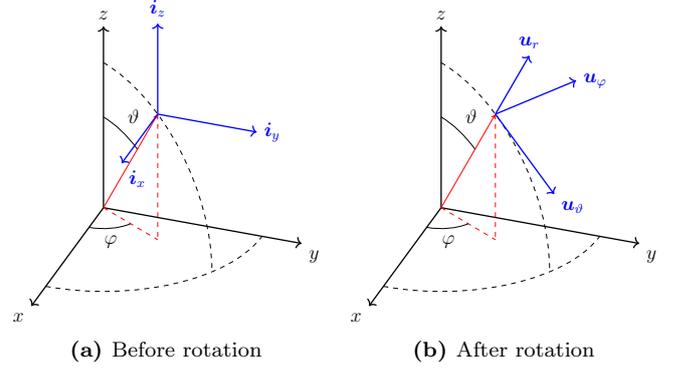(7)

Note that the recurrence schemes (2)–(4) and, correspondingly, the gradient (5) involve SHs of maximum order $N+1$ and the Hessian (6) involves SHs of maximum order $N+2$. The matrices $\boldsymbol{G}_N^x, \boldsymbol{G}_N^y, \boldsymbol{G}_N^z$ of dimensions $(N+1)^2 \times (N+2)^2$ superimpose a shifted combination of SHs of maximum order $N+1$ to obtain the partial derivatives in $x, y, z$ of SHs of maximum order $N$. A MATLAB function that returns the matrices $\boldsymbol{G}_N^x, \boldsymbol{G}_N^y, \boldsymbol{G}_N^z$ is provided online[1].

If multiple observations of $\boldsymbol{\gamma}_N$ are available, the algorithm can be modified to search for roots of the noise subspace. The objective function is then the one of the MUSIC algorithm, such that Newton's method can be applied in direction-of-arrival estimation to avoid the computationally expensive grid search [12].

The Hessian (6) containing all second-order derivatives in $x, y, z$ is singular for directions on the unit sphere, where a coordinate axis is orthogonal to the surface of the unit sphere, i.e., for spherical directions with azimuth angles $\varphi \in \{0°, 90°, 180°, 270°\}$ or with zenith angles $\vartheta \in \{0°, 180°\}$. A non-singular $2 \times 2$ Hessian in the two tangential angular-coordinate directions $\boldsymbol{u}_\varphi$ and $\boldsymbol{u}_\vartheta$,

$$\tilde{\boldsymbol{H}} = \begin{bmatrix} \tilde{h}_{\varphi\varphi} & \tilde{h}_{\varphi\vartheta} \\ \tilde{h}_{\vartheta\varphi} & \tilde{h}_{\vartheta\vartheta} \end{bmatrix} = \boldsymbol{M}^{\mathrm{T}} \boldsymbol{R}^{\mathrm{T}} \boldsymbol{H} \boldsymbol{R} \boldsymbol{M},$$
(8)

---

[1] https://git.iem.at/thomasdeppisch/
real-sh-recurrence-relations



**Figure 1:** Rotation of the Cartesian unit vectors $\boldsymbol{i}_x, \boldsymbol{i}_y, \boldsymbol{i}_z$ to the spherical unit vectors $\boldsymbol{u}_\varphi, \boldsymbol{u}_\vartheta, \boldsymbol{u}_r$ at a point on the surface of the unit sphere.

is obtained via the Cartesian identity vectors $[\boldsymbol{i}_x, \boldsymbol{i}_y, \boldsymbol{i}_z] = \boldsymbol{I}$, rotated to the azimuthal, zenithal, and radial directions, using $\boldsymbol{R} = [\boldsymbol{u}_\varphi, \boldsymbol{u}_\vartheta, \boldsymbol{u}_r]$, $\boldsymbol{u}_r = \boldsymbol{\theta}$,

$$\boldsymbol{R} = \begin{bmatrix} -\sin(\varphi) & \cos(\varphi)\cos(\vartheta) & \cos(\varphi)\sin(\vartheta) \\ \cos(\varphi) & \sin(\varphi)\cos(\vartheta) & \sin(\varphi)\sin(\vartheta) \\ 0 & -\sin(\vartheta) & \cos(\vartheta) \end{bmatrix}, \quad (9)$$

and projection onto the two tangential dimensions with

$$\boldsymbol{M} = \begin{bmatrix} 1 & 0 \\ 0 & 1 \\ 0 & 0 \end{bmatrix}.$$
(10)

The rotation from Cartesian to spherical unit vectors is shown in Fig. 1.

The $2 \times 2$ Hessian $\tilde{\boldsymbol{H}}$ replacing $\boldsymbol{H}$ permits a tangential Newton update that is not inherently rank-deficient,

$$\boldsymbol{\theta}_{k+1} = \boldsymbol{\theta}_k - \boldsymbol{R} \boldsymbol{M} \tilde{\boldsymbol{H}}^{-1} \boldsymbol{M}^{\mathrm{T}} \boldsymbol{R}^{\mathrm{T}} \boldsymbol{g}, \quad (11)$$
$$\boldsymbol{\theta}_{k+1} \leftarrow \boldsymbol{\theta}_{k+1} / \|\boldsymbol{\theta}_{k+1}\|.$$

After convergence, the resulting Hessian can be analyzed to exclude saddle points, i.e., points where the Hessian neither indicates a minimum by being positive definite $\tilde{\boldsymbol{H}} \succ 0$ nor a maximum by being negative definite $\tilde{\boldsymbol{H}} \prec 0$.

## Directivity Pattern Resynthesis

Each peak in the directivity pattern is fully characterized by its direction $\boldsymbol{\theta}$ as location, the local amplitude $a$, and the local Hessian $\tilde{\boldsymbol{H}}$ describing two-dimensional, tangential curvature: its eigenvector $\boldsymbol{v}_>$ of the larger absolute eigenvalue $\sigma_>$ describes the semi-major axis of curvature, and the other one $\boldsymbol{v}_<$ with smaller absolute eigenvalue $\sigma_<$ describes the semi-minor axis of curvature. Drawing a circle on both tangential axes $\boldsymbol{v}_>$ and $\boldsymbol{v}_<$ scaled by $a/\sigma_>$ and $a/\sigma_<$, respectively, permits to characterize any lobe by an ellipse, see Fig. 2. Consequently, describing any lobe by $\{\boldsymbol{\theta}, a, \tilde{\boldsymbol{H}}\}$ facilitates novel ways to resynthesize sound source directivities. We propose a minimum-norm directivity synthesis fulfilling linear equality constraints of such a parametric radiation-lobe description.

### Minimum-Norm Directivity Patterns
To be able to formulate an optimization problem with linear equality constraints on $\boldsymbol{\gamma}_N$, it needs to be factored

out from the definition of the Hessian $\boldsymbol{H}$ (6),

$$\mathring{\boldsymbol{H}} = \begin{bmatrix} \mathring{\boldsymbol{h}}_{xx}^{\mathrm{T}} & \mathring{\boldsymbol{h}}_{yx}^{\mathrm{T}} & \mathring{\boldsymbol{h}}_{zx}^{\mathrm{T}} \\ \mathring{\boldsymbol{h}}_{xy}^{\mathrm{T}} & \mathring{\boldsymbol{h}}_{yy}^{\mathrm{T}} & \mathring{\boldsymbol{h}}_{zy}^{\mathrm{T}} \\ \mathring{\boldsymbol{h}}_{xz}^{\mathrm{T}} & \mathring{\boldsymbol{h}}_{yz}^{\mathrm{T}} & \mathring{\boldsymbol{h}}_{zz}^{\mathrm{T}} \end{bmatrix} , \tag{12}$$

where

$$\mathring{\boldsymbol{h}}_{\alpha\beta}^{\mathrm{T}} = \boldsymbol{y}_{N+2}^{\mathrm{T}} \boldsymbol{G}_{N+1}^{\alpha\mathrm{T}} \boldsymbol{G}_N^{\beta\mathrm{T}} \tag{13}$$

is the same as $h_{\alpha\beta}$ (7) except $\boldsymbol{\gamma}_N$ is factored out. After expanding the matrix product defining $\tilde{\boldsymbol{H}}$ (8), $\boldsymbol{\gamma}_N$ can again be factored out and the half-vectorized Hessian $\tilde{\boldsymbol{h}} = \mathrm{vech}(\tilde{\boldsymbol{H}})$ containing the lower triangular entries of $\tilde{\boldsymbol{H}}$ can be re-expressed as $\tilde{\boldsymbol{h}} = \boldsymbol{A}\boldsymbol{\gamma}_N$, where

$$\boldsymbol{A} = \begin{bmatrix} r_{11} \left( \mathring{\boldsymbol{h}}_{xx}^{\mathrm{T}} r_{11} + \mathring{\boldsymbol{h}}_{xy}^{\mathrm{T}} r_{21} + \mathring{\boldsymbol{h}}_{xz}^{\mathrm{T}} r_{31} \right) + r_{21} \left( \mathring{\boldsymbol{h}}_{yx}^{\mathrm{T}} r_{11} + \mathring{\boldsymbol{h}}_{yy}^{\mathrm{T}} r_{21} + \mathring{\boldsymbol{h}}_{yz}^{\mathrm{T}} r_{31} \right) + r_{31} \left( \mathring{\boldsymbol{h}}_{zx}^{\mathrm{T}} r_{11} + \mathring{\boldsymbol{h}}_{zy}^{\mathrm{T}} r_{21} + \mathring{\boldsymbol{h}}_{zz}^{\mathrm{T}} r_{31} \right) \\ r_{12} \left( \mathring{\boldsymbol{h}}_{xx}^{\mathrm{T}} r_{11} + \mathring{\boldsymbol{h}}_{xy}^{\mathrm{T}} r_{21} + \mathring{\boldsymbol{h}}_{xz}^{\mathrm{T}} r_{31} \right) + r_{22} \left( \mathring{\boldsymbol{h}}_{yx}^{\mathrm{T}} r_{11} + \mathring{\boldsymbol{h}}_{yy}^{\mathrm{T}} r_{21} + \mathring{\boldsymbol{h}}_{yz}^{\mathrm{T}} r_{31} \right) + r_{32} \left( \mathring{\boldsymbol{h}}_{zx}^{\mathrm{T}} r_{11} + \mathring{\boldsymbol{h}}_{zy}^{\mathrm{T}} r_{21} + \mathring{\boldsymbol{h}}_{zz}^{\mathrm{T}} r_{31} \right) \\ r_{12} \left( \mathring{\boldsymbol{h}}_{xx}^{\mathrm{T}} r_{12} + \mathring{\boldsymbol{h}}_{xy}^{\mathrm{T}} r_{22} + \mathring{\boldsymbol{h}}_{xz}^{\mathrm{T}} r_{32} \right) + r_{22} \left( \mathring{\boldsymbol{h}}_{yx}^{\mathrm{T}} r_{12} + \mathring{\boldsymbol{h}}_{yy}^{\mathrm{T}} r_{22} + \mathring{\boldsymbol{h}}_{yz}^{\mathrm{T}} r_{32} \right) + r_{32} \left( \mathring{\boldsymbol{h}}_{zx}^{\mathrm{T}} r_{12} + \mathring{\boldsymbol{h}}_{zy}^{\mathrm{T}} r_{22} + \mathring{\boldsymbol{h}}_{zz}^{\mathrm{T}} r_{32} \right) \end{bmatrix} \tag{14}$$

and $r_{ij}$ is the $i$th row and $j$th column element of $\boldsymbol{R}$.

A minimum-norm directivity pattern that is constrained by the direction $\boldsymbol{\theta}_k$, amplitude $a_k$ and half-vectorized Hessian $\tilde{\boldsymbol{h}}_k = \mathrm{vech}(\tilde{\boldsymbol{H}}_k)$ of each of the $K$ radiation lobes can now be expressed by the linearly-constrained optimization problem

$$\begin{aligned} \min \quad & \|\boldsymbol{\gamma}_N\|_2^2 \tag{15} \\ \text{s.t.} \quad & \boldsymbol{A}_k \boldsymbol{\gamma}_N = \tilde{\boldsymbol{h}}_k && \forall k \in [1, K] \\ & \boldsymbol{y}_N^{\mathrm{T}}(\boldsymbol{\theta}_k) \boldsymbol{\gamma}_N = a_k && \forall k \in [1, K]. \end{aligned}$$

All $K$ Hessian constraints and all $K$ amplitude constraints can be combined into a single equality constraint $\boldsymbol{\Gamma}\boldsymbol{\gamma}_N = \boldsymbol{\rho}$ by stacking all $\boldsymbol{A}_k$ of dimension $3 \times (N+1)^2$ and all $\boldsymbol{y}_N^{\mathrm{T}}(\boldsymbol{\theta}_k)$ of dimension $1 \times (N+1)^2$ in the combined $4K \times (N+1)^2$ matrix $\boldsymbol{\Gamma}$ and all $\tilde{\boldsymbol{h}}_k$ and $a_k$ in the combined $4K \times 1$ vector $\boldsymbol{\rho}$. The optimum solution $\boldsymbol{\gamma}_N^*$ is then obtained by using a Lagrange multiplier [12]

$$\boldsymbol{\gamma}_N^* = \boldsymbol{\Gamma}^{\mathrm{T}}(\boldsymbol{\Gamma}\boldsymbol{\Gamma}^{\mathrm{T}})^{-1}\boldsymbol{\rho} . \tag{16}$$

**Resynthesis of a Simplified Pattern**
We propose and evaluate two ways of resynthesizing a simplified directivity pattern: i) The resynthesized pattern can be assembled from a subset of the found radiation lobes, e.g. the most prominent ones, and ii), the SH order of the resynthesized pattern can be reduced. Resynthesis based on a reduced number of peaks is achieved by only including the peaks of interest in the equality constraints of the optimization problem (15). Reduction of the SH resynthesis order is achieved by reducing the order $N$ in the optimization problem. However, reducing the resynthesis order without modifying the Hessian constraint can in many cases lead to an infeasible solution set as it is not generally possible to reproduce the peak curvature of a high-order SH pattern with a lower-order SH pattern. In such cases, we propose a relaxation of the Hessian constraint.

As derived in [12], the curvature of a single order-$N$ SH beam $\boldsymbol{y}_N(\boldsymbol{\theta})$ follows

$$\frac{\partial^2}{\partial \vartheta^2} \sum_{n=0}^{N} \sum_{m=-n}^{n} Y_n^m(0,0) Y_n^m(0, \vartheta) \Big|_{\vartheta=0} = -\frac{N(N+1)^2(N+2)}{16\pi} . \tag{17}$$
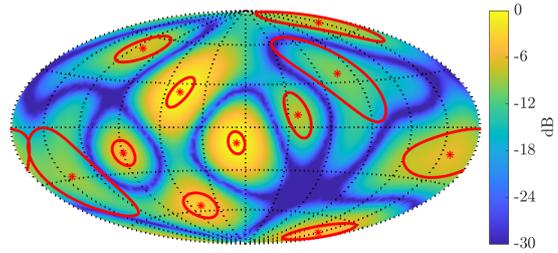


**Figure 2:** Map projection of the magnitude of the randomly generated directivity pattern. Red asterisks indicate 11 peak locations found via Newton's method and red ellipses show the corresponding tangential curvature at each peak. A balloon plot of the same directivity is shown in Fig. 3a.

To relax the Hessian constraint, we propose to reweight the entries of the Hessian using the ratio of the curvature of the low-order peak to the curvature of the high-order peak

$$\kappa = \frac{\tilde{N}(\tilde{N}+1)^2(\tilde{N}+2)}{N(N+1)^2(N+2)} , \tag{18}$$

where $\tilde{N}$ and $N$ are the maximum SH orders of the low-order and higher-order directivity, respectively. The Hessian at the peak of a low-order SH beam $\boldsymbol{y}_{\tilde{N}}(\boldsymbol{\theta})$ can be obtained from the Hessian at the peak of a high-order SH beam $\boldsymbol{y}_N(\boldsymbol{\theta})$ via a multiplication by $\kappa$. By multiplication of the target Hessians $\tilde{\boldsymbol{h}}_k$ in the constraints of (15) by $\kappa$, the constraints are relaxed and lower-order patterns are resynthesized with lower peak curvature.
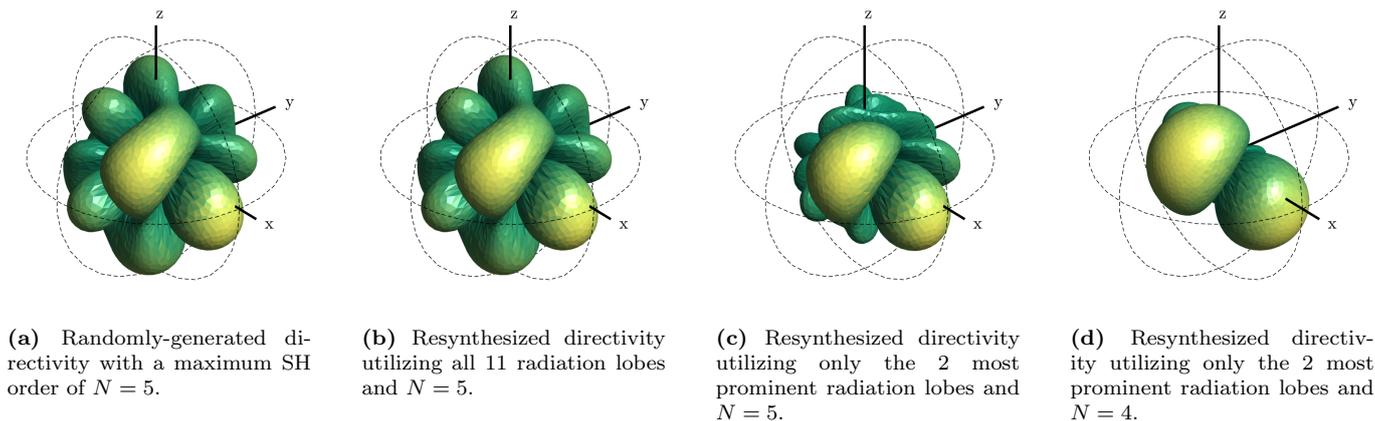
Depending on the application, different normalizations of the simplified minimum-norm patterns can be beneficial. A constant diffuse-field energy is achieved by matching the SH vector norm of the simplified, possibly lower-order pattern $\boldsymbol{\gamma}_{\tilde{N}}$ with the one of the original, higher-order pattern $\boldsymbol{\gamma}_N$, $\hat{\boldsymbol{\gamma}}_{\tilde{N}} = \boldsymbol{\gamma}_{\tilde{N}} \|\boldsymbol{\gamma}_N\| / \|\boldsymbol{\gamma}_{\tilde{N}}\|$. Alternatively, a constant ratio of peak curvature to amplitude via multiplication by $\kappa$ retains the shape of the radiation lobes after SH order reduction, $\hat{\boldsymbol{\gamma}}_{\tilde{N}} = \kappa \boldsymbol{\gamma}_{\tilde{N}}$.

## Case Study: Analysis and Resynthesis of a Random Directivity Pattern
We provide a qualitative insight into the workings of the proposed method by exemplarily analyzing and resynthesizing a randomly generated directivity of order $N = 5$. The magnitude of the generated directivity pattern is shown as a map projection in Fig. 2 and as balloon plot in Fig. 3a. Fig. 2 additionally shows 11 peak locations that were found by Newton's method and are indicated by red asterisks. The tangential curvature of the peaks is indicated by red ellipses.

As evident from the map projection and the balloon plot, the directivity exhibits two prominent radiation lobes. Using the proposed radiation lobe decomposition and the minimum-norm directivity resynthesis, we exemplarily investigate two ways of simplifying the overall directivity pattern while accurately reproducing the two prominent radiation lobes.

Fig. 3 shows balloon plots of the original directivity pat-

**(a)** Randomly-generated directivity with a maximum SH order of $N = 5$.

**(b)** Resynthesized directivity utilizing all 11 radiation lobes and $N = 5$.

**(c)** Resynthesized directivity utilizing only the 2 most prominent radiation lobes and $N = 5$.

**(d)** Resynthesized directivity utilizing only the 2 most prominent radiation lobes and $N = 4$.

**Figure 3:** Balloon plots of the magnitude of the randomly generated directivity and 3 resynthesized directivities.

tern and three resynthesized, minimum-norm directivity patterns. All balloon plots were compiled with a dynamic range of 40 dB. The resynthesized directivity in Fig. 3b utilizes all 11 found peak locations, amplitudes and tangential curvatures and a maximum SH order of $N = 5$. It recreates the original directivity pattern perfectly. Fig. 3c and 3d show simplified directivities that only resynthesize the two most prominent radiation lobes. The directivity of Fig. 3c uses a maximum SH order of $N = 5$ and reproduces the radiation lobes accurately in direction, magnitude and curvature. The directivity in Fig. 3d utilizes a reduced maximum SH order of $N = 4$ and reproduces the radiation lobes in direction and relative magnitude, while the global magnitude is modified according to the proposed normalization via multiplication by $\kappa$. Due to the relaxation of the Hessian constraint, the reproduced curvature of the radiation lobes is lower than in the original directivity.

## Conclusion

With the radiation lobe decomposition, we proposed a comprehensive parametric description of directivity patterns that reveals valuable information about sound source directivities. Newton's method determines the peaks in the directivity accurately and efficiently. Based on the novel parametric description of the radiation lobes, the proposed minimum-norm resynthesis method permits the simplification of the directivity to an arbitrary extent while preserving its main characteristics, which facilitates practical trade-offs between spatial resolution and computational cost.

## References

[1] F. Otondo and J. H. Rindel, "The influence of the directivity of musical instruments in a room," *Acta Acustica united with Acustica*, vol. 90, no. 6, pp. 1178–1184, 2004.

[2] B. I. Dalenbäck, M. Kleiner, and P. Svensson, "Audibility of changes in geometric shape, source directivity, and absorptive treatment - experiments in auralization," *AES: Journal of the Audio Engineering Society*, vol. 41, no. 11, pp. 905–913, 1993.

[3] M. Frank and M. Brandner, "Perceptual Evaluation of Spatial Resolution in Directivity Patterns," in *Fortschritte der Akustik – DAGA*, 2019.

[4] K. Enge, M. Frank, and R. Höldrich, "Listening experiment on the plausibility of acoustic modeling in virtual reality," in *Fortschritte der Akustik – DAGA*, 2020.

[5] M. Pollow, G. K. Behler, and B. Masiero, "Measuring Directivities Of Natural Sound Sources With A Spherical Microphone Array," in *Proc. Ambisonics Symposium*, 2009.

[6] B. Rafaely, "Spatial alignment of acoustic sources based on spherical harmonics radiation analysis," *Proc. of the 4th International Symposium on Communications, Control and Signal Processing*, 2010.

[7] D. Deboy and F. Zotter, "Acoustic center and orientation analysis of sound-radiation recorded with a surrounding spherical microphone array," in *Proc. of the 2nd International Symposium on Ambisonics and Spherical Acoustics*, 2010.

[8] I. Ben Hagai, M. Pollow, M. Vorländer, and B. Rafaely, "Acoustic centering of sources measured by surrounding spherical microphone arrays," *The Journal of the Acoustical Society of America*, vol. 130, no. 4, pp. 2003–2015, 2011.

[9] F. Zagala and F. Zotter, "Idea for Sign-Change Retrieval in Magnitude Directivity Patterns," in *Fortschritte der Akustik – DAGA*, 2019.

[10] G. Götz and V. Pulkki, "Simplified Source Directivity Rendering in Acoustic Virtual Reality using the Directivity Sample Combination," in *Proc. of the 147th Conv. of the Audio Eng. Soc.*, 2019.

[11] N. A. Gumerov and R. Duraiswami, "Fast, exact, and stable computation of multipole translation and rotation coefficients for the 3-d helmholtz equation," *UMIACS Technical Reports*, vol. 44, p. 45, 2001.

[12] T. Deppisch, "Multi-Direction Analysis in Ambisonics," Master's thesis, University of Music and Performing Arts, Graz, 2020.